RSC Advances

PAPER

View Article Online
View Journal | View Issue

Cite this: *RSC Adv.*, 2021, **11**, 28375

Mesoporous $MnFe_2O_4$ magnetic nanoparticles as a peroxidase mimic for the colorimetric detection of urine glucose†

Ke Liu,‡ Jiaxing Su,‡ Jiangong Liang and Yuan Wu*

Mesoporous $MnFe_2O_4$ magnetic nanoparticles (m$MnFe_2O_4$ MNPs) were prepared with a one-step synthesis method and characterized to possess intrinsic peroxidase-like activity, and had obvious advantages over other peroxidase nanozymes in terms of high catalytic affinity, high stability, mono-dispersion, easy preparation, and quick separation. The m$MnFe_2O_4$ MNPs were used as a colorimetric sensor for indirect sensing of urine glucose based on the sensing principle that H_2O_2 can be produced from glucose oxidation catalyzed by glucose oxidase (GOx), and under the catalysis of the m$MnFe_2O_4$ MNPs nanozyme, H_2O_2 can oxidize 3,3′,5,5′-tetramethylbenzidine (TMB) to produce a blue color in a few minutes. This sensor is simple, cheap, sensitive, and specific to glucose detection with a detection limit of 0.7 μM, suggesting its potential for on-site glucose detection.

Received 14th July 2021
Accepted 4th August 2021

DOI: 10.1039/d1ra05396e

rsc.li/rsc-advances

1. Introduction

Glucose, an important energy source in the human body, participates in many physiological and pathological functions. Irregular glucose metabolism in urine is an early warning of health problems,[1] such as diabetes, a metabolic disease characterized by high glucose in blood and urine, resulting in serious damage to the human body,[2] suggesting the importance of early and accurate detection of urine glucose for health monitoring. For this purpose, various biosensors have been invented for glucose detection, including electrochemical[3–7] and fluorescence[8–10] techniques. However, most of these biosensors are complicated in construction and sophisticated in equipment, indicating the necessity to develop a simple, low cost and easy-to-detect method for on-site monitoring of the glucose level.

Another indirect method for evaluating glucose level is to detect H_2O_2 generated from glucose oxidase catalyzed by glucose oxidase (GOx).[11] Horseradish peroxidase (HRP), a natural enzyme catalyzing the oxidation of 3,3′,5,5′-tetramethylbenzidine (TMB) or other substrates by H_2O_2, is the enzyme most commonly used as a diagnostic kit for H_2O_2 sensing.[12] However, the activity of HRP is not stable in a harsh environment (such as in extreme pH medium, organic solvents, and high temperature), and preparing pure HRP is time-consuming and expensive,[13] thereby limiting the practical application of HRP as a natural enzyme. To solve these problems, an increasing number of scientists have turned their attention to the construction of efficient enzyme mimics. Since Yan *et al.* first reported Fe_3O_4 magnetic nanoparticles (NPs) as peroxidase mimics (termed as "nanozyme"),[14] many other nanozymes have been developed and applied for indirect glucose detection,[15–18] such as ZnO NPs,[19] V_2O_5 nanowires,[20] Au NPs,[21] Pt NPs,[22] and Pd NPs.[23] However, the enzyme-like activity of most nanozymes can be easily affected by additional coating or modification. Therefore, it is still necessary to develop new nanozymes with high performance.

In the past few years, spinel ferrites (MFe_2O_4, M = Zn, Co, Ni, Cd, Mn) have attracted increasing attention due to their wide application in the fields of magnetic materials, energy, environmental protection, biomedicine, and catalytic application.[24–27] Their chemical and physical properties can be effectively regulated by tuning the shape, size, and morphology.[28] Thus, ferrite nanomaterials with different morphologies have been successfully prepared, such as homogeneous hollow microspheres of spinel ferrites,[29] porous "timber-like" $ZnFe_2O_4$ structures[30] and $MnFe_2O_4$ nanomaterials with nano-octahedron, nano-sheet or nano-wire morphologies.[31] Interestingly, the $MnFe_2O_4$ nanomaterials showed high morphology-dependent oxidase-like activity, with a considerably higher oxidase-like activity for the $MnFe_2O_4$ nanomaterials with a nano-octahedron morphology than those with a nano-sheet or nano-wire morphology. Therefore, the tunable morphology-dependent enzyme-like property of the spinel ferrites has attracted the attention of an increasing number of researchers.

State Key Laboratory of Agricultural Microbiology, College of Science, Huazhong Agricultural University, Wuhan 430070, China. E-mail: yuanwu@mail.hzau.edu.cn; Fax: +86-27-8728-2133; Tel: +86-27-8728-3712

† Electronic supplementary information (ESI) available. See DOI: 10.1039/d1ra05396e

‡ These authors contributed equally to this work.

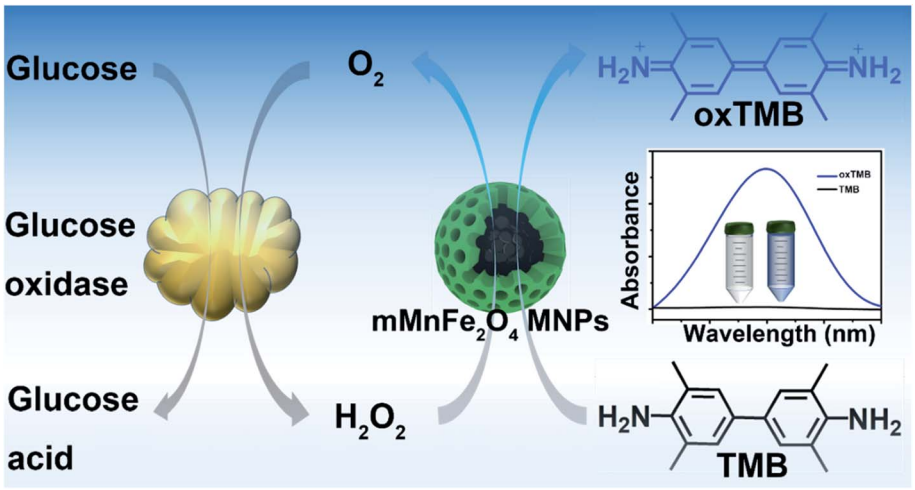

Scheme 1 Schematic illustration of glucose detection with glucose oxidase (GOx) and $mMnFe_2O_4$ MNPs-catalyzed system.

Here, we report the one-step green-synthesis of mesoporous $MnFe_2O_4$ magnetic nanoparticles ($mMnFe_2O_4$ MNPs) with high intrinsic peroxidase activity, uniform distribution, high stability, and rapid separation. As shown in Scheme 1, H_2O_2 can be generated from glucose oxidation catalyzed by GOx, and under the catalysis of the $mMnFe_2O_4$ MNPs nanozyme, TMB can be oxidized by H_2O_2 to produce a blue color observable with the naked eye in a few minutes. Based on this principle, we developed a colorimetric sensor for glucose detection, which showed great potential for point-of-care monitoring of urine glucose due to its easy preparation, low cost, and quick detection.

2. Experimental section

2.1 Materials

Sodium acetate (NaAc), ferric chloride ($FeCl_3 \cdot 6H_2O$), manganous dichloride ($MnCl_2 \cdot 4H_2O$), ethylene glycol (EG), hydrogen peroxide (H_2O_2), 3,3′,5,5′-tetramethylbenzidine (TMB), fructose, lactose, and maltose were purchased from Sinopharm Chemical Reagent Co. Ltd (Shanghai, China), glucose from Sigma-Aldrich, glucose oxidase (GOx, 10 KU) from Aladdin. All other chemicals were of analytical grade and used without further purification. Deionized water was used throughout the experiment.

2.2 Apparatus and characterization

A JEOL JEM-2010FEF transmission electron microscope (TEM) and a JSM-7900F scanning electron microscope (SEM) were used for measuring the morphology and size of $mMnFe_2O_4$ MNPs. The X-ray diffraction (XRD) pattern of $mMnFe_2O_4$ MNPs was obtained with a Shimadzu XRD-7000 diffractometer with Cu Kα radiation ($\lambda = 0.154056$). The zeta potential and size of $mMnFe_2O_4$ MNPs were measured with a Malvern Nano-ZS90 apparatus. Energy dispersive X-ray spectroscopy (EDS) was performed on an Oxford X-max 80 T. X-ray photoelectron spectra (XPS) were acquired using an ESCALAB 250Xi electron spectrometer. The spectra were measured using Al Kα radiation (12.5 kV, 400 W) in a chamber with a base pressure of 8×10^{-8} Pa. UV-Vis spectra were collected using a Shimadzu UV-2450 spectrophotometer.

2.3 Synthesis of $mMnFe_2O_4$ MNPs

The $mMnFe_2O_4$ MNPs were synthesized with a solvothermal method as previously reported with small modifications.[32] Briefly, NaAc (2.7 g) was first completely dissolved in EG (30 mL) under ultrasonication for 10 min, followed by adding $MnCl_2 \cdot 4H_2O$ and $FeCl_3 \cdot 6H_2O$ at a molar ratio of 1 : 2. Next, the mixture was transferred into a Teflon autoclave and sealed to heat overnight at 180 °C. After cooling to room temperature naturally, the $mMnFe_2O_4$ MNPs were obtained with magnet, followed by three washes with water and ethanol and drying at 30 °C. Finally, the dried $mMnFe_2O_4$ MNPs were stored at room temperature for further use.

2.4 Peroxidase activity, reaction-rate factors and steady-state kinetics

The peroxidase activity of $mMnFe_2O_4$ MNPs was studied using TMB as the substrate. Briefly, $mMnFe_2O_4$ MNPs (10 μg mL^{-1}) were quickly mixed with 2.0 mL solution of TMB (400 μM) and H_2O_2 (20 mM) in citric buffer (25 mM, pH 4.0), the absorbance at 652 nm was recorded. Similarly, the factors affecting the rate of catalytic reaction, such as pH, temperature, reaction time, salt concentration, H_2O_2 concentration, and steady-state kinetics, were investigated using TMB as the substrate. Finally, the initial rates were calculated from the plot of absorbance *versus* time.

2.5 Glucose sensing

For glucose sensing, 20 μL of GOx (10 mg mL^{-1}, pH = 7) was first mixed separately with 180 μL of glucose solution at different concentration (0.0, 0.5, 2.5, 5.0, 10.0, 16.0, 50.0, 100.0, 500.0, 1000.0 μM) (pH = 7), and incubated at 37 °C for 30 min. Then, the mixture was supplemented with 1770 μL of citric

buffer (25 mM, pH 4.0), 10 μL of $mMnFe_2O_4$ MNPs (2 mg mL^{-1}) and 20 μL TMB solution (40 mM). After incubation at 37 °C for 30 min, the absorbance of the resulting solution was measured at 652 nm. Meanwhile, the control experiments were performed using maltose, lactose, and fructose to replace glucose in a similar way.

3. Results and discussion

3.1 Characterization of $mMnFe_2O_4$ MNPs

Fig. 1 shows the SEM and TEM images of $mMnFe_2O_4$ MNPs. In the SEM and TEM images, $mMnFe_2O_4$ MNPs were seen to present uniform nanocrystals with a size of nearly 180 nm and a well-defined meso-structure. Fig. S1,† shows the dynamic light scattering (DLS) size distribution of $mMnFe_2O_4$ MNPs. In Fig. S2,† the EDS result showed the existence of Mn, Fe and O elements. The nanoparticles were further characterized by X-ray photoelectron spectroscopy (XPS) (Fig. S3†), and the XPS results are consistent with the previous reports.[31] The above results confirmed that successful synthesis of $mMnFe_2O_4$ nanoparticles.

The structure of $mMnFe_2O_4$ nanoparticles was investigated by FT-IR (Fig. S4†) and XRD (Fig. S5†). All the diffraction peaks are consistent with the FCC structure of $mMnFe_2O_4$ with high crystallinity (JCPDS card no. 74-2403).[33] The porous structure of the nanocrystals was investigated by N_2 adsorption–desorption analysis (Fig. S6a†). The mesopore size was shown to be about 7.6 nm from the HK pore size distribution curve (Fig. S6b†), and the surface area was calculated to be 53.4 $m^2\ g^{-1}$. The magnetic property of $mMnFe_2O_4$ MNPs was characterized by field dependent magnetization (Fig. S7†), and $mMnFe_2O_4$ MNPs were shown to possess superparamagnetic property with 70 emu g^{-1} of maximum saturation magnetization (M_s) value, which is almost comparable to the M_s value of Fe_2O_3 nanoparticles.[34]

3.2 Peroxidase-like activity of $mMnFe_2O_4$ MNPs

After treatment with $mMnFe_2O_4$ MNPs and H_2O_2, the colorless TMB solution rapidly turned blue, with the blue color from the oxidized TMB product (oxTMB). In, Fig. 2a, the UV-vis absorbance of oxTMB at 652 nm was seen to be obviously enhanced in the mixture of $mMnFe_2O_4$ MNPs + TMB + H_2O_2. However, neither H_2O_2 nor $mMnFe_2O_4$ MNPs alone can efficiently oxidize TMB to produce a blue color. Therefore, TMB can be oxidized by H_2O_2 under the catalysis of $mMnFe_2O_4$ MNPs, which is also the case for horseradish peroxidase (HRP). These results indicated that $mMnFe_2O_4$ MNPs may possess an intrinsic peroxidase-like activity, which was further characterized by using other peroxidase substrates, such as 2,2-azino-bis (3-ethylbenzothiazoline-6-sulfonic acid) (ABTS) and *o*-phenylenediamine (OPD), to replace TMB (Fig. 2b), and $mMnFe_2O_4$ MNPs were shown to possess a broad peroxidase-like activity. Moreover, in Fig. S8,† the peroxidase-like activity was observed to be caused by $mMnFe_2O_4$ MNPs rather than ions leached from $mMnFe_2O_4$ MNPs in acidic solution.

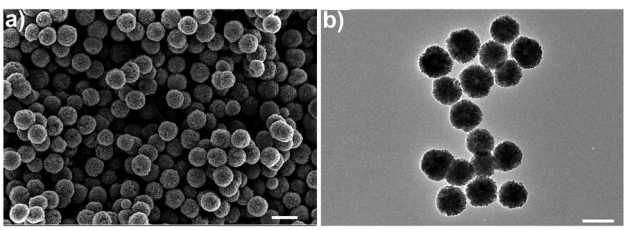

Fig. 1 (a) SEM image (scale bar 300 nm), (b) TEM image (scale bar 200 nm). For specificity test, the system was incubated with interference ions (Cd^{2+}, Pb^{2+}, Zn^{2+}, Cu^{2+}, Fe^{3+}, K^+, Na^+, As^{3+}, Cr^{3+}, Mn^{2+}, Ag^+, Ca^{2+}, Ba^{2+}, Mg^{2+}; Cl^-, Br^-, NO_3^-, SO_4^{2-}, CO_3^{2-}, F^-, OH^-) at a high concentration of 500 μM, and the other procedures were the same as described above. For urine sample tests, urine samples were collected and filtered through a filter with pore size of 0.22 μm, and different concentration of glucose were added as described above. Finally, the absorbance of the samples was measured at 652 nm using a spectrophotometer.

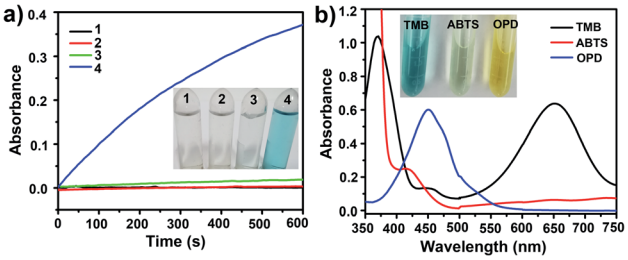

Fig. 2 (a) Feasibility study of H_2O_2 sensing based on the catalytic ability of $mMnFe_2O_4$ MNPs characterized by UV-vis spectroscopy at 652 nm. (1) TMB; (2) $mMnFe_2O_4$ MNPs + TMB; (3) TMB + H_2O_2; (4) $mMnFe_2O_4$ MNPs + TMB + H_2O_2. (b) UV-vis spectra of $mMnFe_2O_4$ MNPs to produce different colors under different substrates (TMB, ABTS and OPD). Inset: the corresponding photographs.

The kinetic mechanism of the peroxidase-like activity of $mMnFe_2O_4$ MNPs was investigated by analyzing apparent steady-state kinetic parameters at varying TMB concentrations (50–800 μM). The typical Michaelis–Menten curves were obtained by measuring the absorbance of TMB at 652 nm for 300 s (Fig. 3a). Michaelis–Menten constant (K_m) and maximum initial velocity (V_{max}) were calculated through Lineweaver–Burk plots (Fig. 3b and c). It was reported the smaller the K_m value, the stronger the affinity between enzyme and substrate.[35] The apparent K_m value for the $mMnFe_2O_4$ MNPs with TMB as the substrate is 0.07 mM^{-1}, which is significantly lower than that of the other catalysts (Table S1†), suggesting higher affinity of $mMnFe_2O_4$ MNPs for TMB. This could be due to the mesoporous structure of $mMnFe_2O_4$ MNPs, which can enhance the up-take of TMB by $mMnFe_2O_4$ MNPs and strengthen the catalytic activity. In Fig. 3d, $mMnFe_2O_4$ MNPs were shown to decompose H_2O_2 to produce ·OH radical, which is consistent with previous report that the catalytic mechanism of nanozymes is to bind and react with H_2O_2 and then release hydroxyl radical (OH) to react with TMB.[36]

3.3 Optimization of experimental conditions

Like natural enzyme HRP, the peroxidase-like activity of $mMnFe_2O_4$ MNPs is dependent on reaction conditions. The

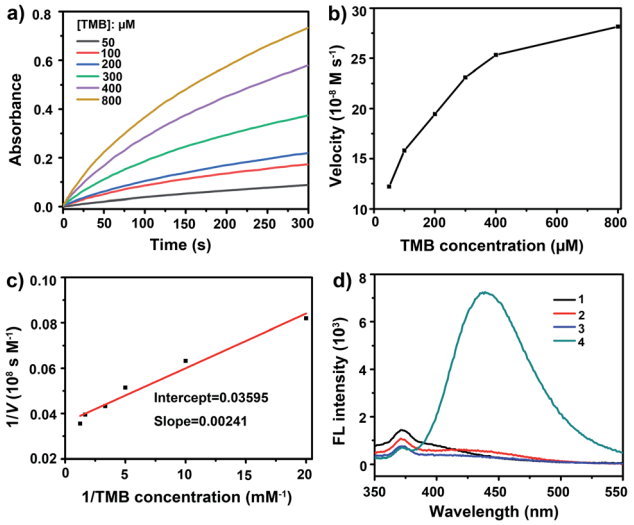

Fig. 3 Steady-state kinetic of peroxidase-like activity of $mMnFe_2O_4$ MNPs. (a) Time-dependent absorbance changes at 652 nm of TMB catalyzed by $mMnFe_2O_4$ MNPs in the presence of TMB at different concentrations; (b) the velocity of reaction changes in the presence of TMB at different concentrations; (c) Lineweaver–Burk plot corresponding to (b). (d) Detecting hydroxyl radical (·OH) with fluorescence spectra of TA in the different mediums. (1) TA; (2) TA + $mMnFe_2O_4$ MNPs; (3) TA + H_2O_2; (4) TA + $mMnFe_2O_4$ MNPs + H_2O_2.

catalytic activity of $mMnFe_2O_4$ MNPs is much higher in acidic solutions (Fig. S9a†). In Fig. S10,† the SEM result showed that the morphology of $mMnFe_2O_4$ MNPs remained almost intact at pH 4.0 for 2 h. Considering the stability and catalytic efficiency of $mMnFe_2O_4$ MNPs, pH 4.0 was defined as the optimal pH value experiment. Meanwhile, the incubation temperature of $mMnFe_2O_4$ MNPs with TMB and H_2O_2 was also investigated and the results are shown in Fig. S9b,† with 37 °C as the optimal temperature. Additionally, the optimal concentration of H_2O_2 was investigated in the range of 0 to 60 mM, and the absorbance at 652 nm obviously increased and reached a plateau at 20 mM (Fig. S9c†), so 20 mM was chosen as the optimal H_2O_2 concentration for further experiments. Similarly, 0.4 mM of TMB (Fig. S9d†) and 10 μg mL^{-1} of $mMnFe_2O_4$ MNPs (Fig. S9e†) were found to the optimal parameters for further experiments. Furthermore, the incubation time of $mMnFe_2O_4$ MNPs with TMB and H_2O_2 was also optimized to achieve the best catalytic activity of the nanozymes (Fig. S9f†), and 15 min was shown as the optimal incubation time. In this study, the optimized experimental conditions consisted of pH 4.0, 37 °C, 20 mM of H_2O_2, 0.4 mM of TMB, 10 μg mL^{-1} of $mMnFe_2O_4$ MNPs, and 15 min of incubation time.

Besides, the enzymatic-like reaction activity of $mMnFe_2O_4$ MNPs was shown not to be affected by adding NaCl (0–0.25 M) to the reaction media (Fig. S11†), confirming the high stability of our nanozymes in NaCl media.

3.4 Application to glucose detection

Since the catalytic activity of $mMnFe_2O_4$ MNPs depends on H_2O_2, H_2O_2 is the main product of glucose oxidation catalyzed by glucose oxidase (GOx). When combined with GOx, the

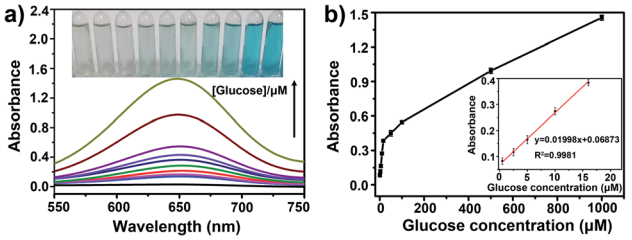

Fig. 4 Biosensing performance of the colorimetric sensor with different glucose concentrations. (a) UV-vis spectra of TMB + $mMnFe_2O_4$ MNPs in the presence of varying concentrations of glucose (from bottom to top: 0.0, 0.5, 2.5, 5.0, 10.0, 16.0, 50.0, 100.0, 500.0, 1000.0 μM). Inset: the corresponding photographs, from left to right. (b) Calibration curve of absorbance at 652 nm *vs.* glucose concentration. Inset: linear relationship of absorbance at 652 nm *vs.* glucose concentration.

$mMnFe_2O_4$ MNPs could be used for glucose detection instead of traditional HRP. Fig. 4a shows the glucose concentration-response curves to the absorbance of oxTMB. The linear range for glucose was from 0.5 to 16.0 μM with a detection limit of 0.7 μM (S/N ≥ 3) (Fig. 4b), which was lower than the detection limit of several previously reported nanozyme-based methods (Table S2†).

3.5 Specificity test

Specificity is important for the application of $mMnFe_2O_4$ MNPs probes. The specificity tests were performed in the presence of common ions (14 cations: Cd^{2+}, Pb^{2+}, Zn^{2+}, Cu^{2+}, Fe^{3+}, K^+, Na^+,

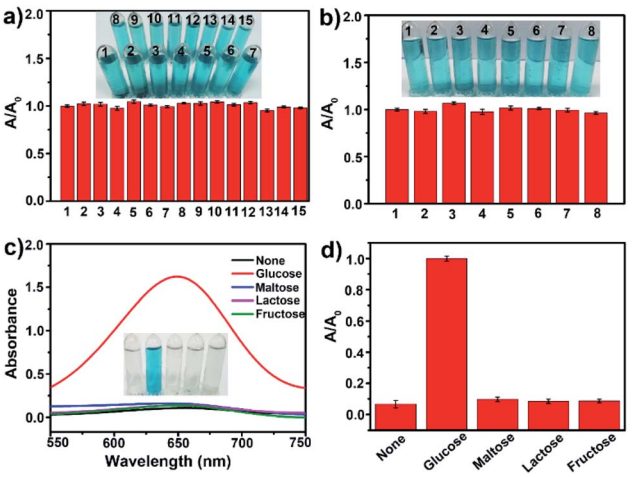

Fig. 5 Specificity tests. (a) The absorbance ratio at 652 nm for interference cations (from 1 to 15: none, Cd^{2+}, Pb^{2+}, Zn^{2+}, Cu^{2+}, Fe^{3+}, K^+, Na^+, As^{3+}, Cr^{3+}, Mn^{2+}, Ag^+, Ca^{2+}, Ba^{2+}, Mg^{2+}). Inset: the corresponding photographs. (b) The absorbance ratio at 652 nm for interference anions (from 1 to 8: none, Cl^-, Br^-, NO_3^-, SO_4^{2-}, CO_3^{2-}, F^-, OH^-). Inset: the corresponding photographs; determination of the specificity of glucose detection. (c) UV-vis spectra of TMB + $mMnFe_2O_4$ MNPs + GOx system in the absence (none) and presence of glucose (1 mM), maltose (10 mM), lactose (10 mM), and fructose (10 mM). Inset: the variation of colors with different solutions. (d) The absorbance ratio at 652 nm for (c). The error bars represent the standard deviation of three measurements.

As^{3+}, Cr^{3+}, Mn^{2+}, Ag^{+}, Ca^{2+}, Ba^{2+}, Mg^{2+}; 7 anions: Cl^{-}, Br^{-}, NO_3^{-}, SO_4^{2-}, CO_3^{2-}, F^{-}, OH^{-}), which did not interfere with H_2O_2 determination (Fig. 5a and b), confirming that the $mMnFe_2O_4$ MNPs probe is specific to H_2O_2. The specificity of the $mMnFe_2O_4$ MNPs nanozyme toward glucose detection was investigated by performing the control experiments using 10 mM of fructose, lactose, and maltose to replace glucose (1 mM). In Fig. 5c and d, the absorbance at 652 nm for glucose was seen to be obviously higher than that of glucose analogues, confirming that the $mMnFe_2O_4$ MNPs nanozyme is highly specific to glucose, probably due to the high affinity of glucose oxidase for glucose.

3.6 Real sample test

The potential of the $mMnFe_2O_4$ MNPs nanozyme for glucose detection was further evaluated by detecting glucose in urine samples from healthy people and a diabetic volunteer. The UV-vis spectra and the colorimetric differentiation are shown in Fig. S12.† According to the calibration curve, the concentration of glucose was 8.2 mM (147.6 mg dL^{-1}) in the diabetic urine, but could hardly be detected in healthy human's urine. The obtained values were further analyzed by spiking different concentrations of glucose into the healthy human's urine and recovering them (Table S3†). Based on the recovery rate and the relative standard deviation (RSD), there was no significant difference between the spiked value and the detected value, indicating the potential of this colorimetric probe for real sample testing.

4. Conclusion

In paper, we reported the synthesis and characterization of the $mMnFe_2O_4$ MNPs with intrinsic peroxidase-like activity as well as their application in colorimetric detection of urine glucose. As a novel peroxidase nanozyme, the $mMnFe_2O_4$ MNPs nanozyme shows several advantages over HRP and other peroxidase nanozymes, such as mesoporous nanostructure, high stability, good dispersibility, excellent separability, and high catalytic efficiency. Based on the reaction mechanism of Scheme 1, we developed a simple, low-cost, highly sensitive, and selective colorimetric method for glucose detection, which shows the practicability of glucose detection in the urine of healthy and diabetic people, suggesting its potential as a simple and useful probe for bioanalysis. The overall results indicate that the $mMnFe_2O_4$ MNPs nanozyme may have broad application prospect as a powerful artificial peroxidase.

Ethical statement

For the human urine experiments, informed consent was obtained from all human subjects. All experiments were performed in compliance with relevant laws or guidelines. All experiments followed institutional guidelines, and were approved by the institutional committee.

Conflicts of interest

There are no conflicts of interest to declare.

Acknowledgements

The authors gratefully acknowledge the financial supports from National Natural Science Foundation of China (21904046, 31772785, 21205043) and the Fundamental Research Funds for the Central Universities (2662018QD042).

References

1 J. Lu, R. F. Bu, Z. L. Sun, Q. S. Lu, H. Jin, Y. Wang, S. H. Wang, L. Li, Z. L. Xie and B. Q. Yang, *Diabetes Res. Clin. Pract.*, 2011, **93**, 179–186.
2 A. Untereiner and L. Y. Wu, *Antioxid. Redox Signaling*, 2017, **28**, 1463–1482.
3 T. Kangkamano, A. Numnuam, W. Limbut, P. Kanatharana and P. Thavarungkul, *Sens. Actuators, B*, 2017, **246**, 854–863.
4 H. Imran, K. Vaishali, S. A. Francy, P. N. Manikandan and V. Dharuman, *Bioelectrochemistry*, 2021, **137**, 107645–107655.
5 Q. Han, H. Wang, D. Wu and Q. Wei, *Biosens. Bioelectron.*, 2021, **173**, 112803–112808.
6 M. Palmer, M. Masikini, L. W. Jiang, J. J. Wang, F. Cummings, J. Chamier, O. Inyang and M. Chowdhury, *J. Alloys Compd.*, 2021, **853**, 156900–156910.
7 X. Wei, J. Guo, H. Lian, X. Sun and B. Liu, *Sens. Actuators, B*, 2021, **329**, 129205–129212.
8 M.-M. Farahani, F. Ghorbani and N. Mosleh, *Spectrochim. Acta, Part A*, 2021, **245**, 118892–118897.
9 Y. L. Ngo, P. L. Nguyen, J. Jana, W. M. Choi, J. S. Chung and S. H. Hur, *Anal. Chim. Acta*, 2021, **1147**, 187–198.
10 K. Kim, H. Kim, E. J. Jo, H. Jang, J. Park, G. Y. Jung and M. G. Kim, *Biosens. Bioelectron.*, 2021, **175**, 112855–112860.
11 A. Tereshchenko, M. Bechelany, R. Viter, V. Khranovskyy, V. Smyntyna, N. Starodub and R. Yakimova, *Sens. Actuators, B*, 2016, **229**, 664–677.
12 D. Sodzel, V. Khranovskyy, V. Beni, A. P. F. Turner, R. Viter, M. O. Eriksson, P. O. Holtz, J. M. Janot, M. Bechelany, S. Balme, V. Smyntyna, E. Kolesneva, L. Dubovskaya, I. Volotovski, A. Ubelis and R. Yakimova, *Microchim. Acta*, 2015, **182**, 1819–1826.
13 J. M. Perez, *Nat. Nanotechnol.*, 2007, **2**, 535–536.
14 L. Z. Gao, J. Zhuang, L. Nie, J. B. Zhang, Y. Zhang, N. Gu, T. H. Wang, J. Feng, D. L. Yang, S. Perrett and X. Y. Yan, *Nat. Nanotechnol.*, 2007, **2**, 577–583.
15 J. Wu, X. Wang, Q. Wang, Z. Lou, S. Li, Y. Zhu, L. Qin and H. Wei, *Chem. Soc. Rev.*, 2019, **48**, 1004–1076.
16 S. Y. Jin, C. Wu, Z. Z. Ye and Y. B. Ying, *Sens. Actuators, B*, 2018, **283**, 18–34.
17 Y. Y. Huang, J. S. Ren and X. G. Qu, *Chem. Rev.*, 2019, **119**, 4357–4412.
18 Y. H. Lin, J. S. Ren and X. G. Qu, *Acc. Chem. Res.*, 2014, **47**, 1097–1105.

19 A. Asati, S. Santra, C. Kaittanis, S. Nath, J. M. Perez and J. Manuel, *Angew Chem. Int. Ed.*, 2010, **121**, 2344–2348.
20 Y. B. Feng, L. Hong, A. L. Liu, W. D. Chen, G. W. Li, W. Chen and X. H. Xia, *Int. J. Environ. Sci. Technol.*, 2015, **12**, 653–660.
21 J. X. Wang, Y. Zhuo, Y. Zhou, H. J. Wang, R. Yuan and Y. Q. Chai, *ACS Appl. Mater. Interfaces*, 2016, **8**, 12968–12975.
22 R. André, F. Natálio, M. Humanes, J. Leppin, K. Heinze, R. Wever, H. C. Schröder, W. E. G. Müller and W. Tremel, *Adv. Funct. Mater.*, 2011, **21**, 501–509.
23 Y. H. Lin, J. S. Ren and X. G. Qu, *Adv. Mater.*, 2014, **26**, 4200–4217.
24 J. Kim, H. R. Cho, H. Jeon, D. Kim, C. Song, N. Lee, S. H. Choi and T. Hyeon, *J. Am. Chem. Soc.*, 2017, **139**, 10992–10995.
25 S. Ida, K. Yamada, T. Matsunaga, H. Hagiwara, Y. Matsumoto and T. Ishihara, *J. Am. Chem. Soc.*, 2010, **132**, 17343–17345.
26 S. H. Xuan, F. Wang, Y. X. Wang, J. C. Yu and K. C. F. Leung, *J. Mater. Chem.*, 2010, **20**, 5086–5094.
27 C. Burda, X. B. Chen, R. Narayanan and M. A. El-Sayed, *Chem. Rev.*, 2005, **105**, 1025–1102.
28 N. Z. Bao, L. M. Shen, Y. H. A. Wang, J. X. Ma, D. Mazumdar and A. Gupta, *J. Am. Chem. Soc.*, 2009, **131**, 12900–12901.
29 Z. M. Li, X. Y. Lai, H. Wang, D. Mao, X. J. Xing and D. Wang, *J. Phys. Chem. C*, 2009, **113**, 2792–2797.
30 M. Wang, Z. H. Ai and L. Z. Zhang, *J. Phys. Chem. C*, 2008, **112**, 13163–13170.
31 A. A. Vernekar, T. Das, S. Ghosh and G. Mugesh, *Chem.–Asian J.*, 2016, **11**, 72–76.
32 X. Y. Long, J. Y. Li, D. Sheng and H. Z. Lian, *Talanta*, 2017, **166**, 36–45.
33 M. A. Peluso, L. A. Gambaro, E. Pronsato, D. Gazzoli, H. J. Thomas and J. E. Sambeth, *Catal. Today*, 2008, **133**, 487–492.
34 S. Laurent, D. Forge, M. Port, A. Roch, C. Robic, L. V. Elst and R. N. Muller, *Chem. Rev.*, 2008, **108**, 2064–2110.
35 Y. Liu, D. L. Purich, C. C. Wu, Y. Wu, T. Chen, C. Cui, L. Q. Zhang, S. Cansiz, W. J. Hou, Y. Y. Wang, S. Y. Yang and W. H. Tan, *J. Am. Chem. Soc.*, 2015, **137**, 14952–14958.
36 L. Su, J. Feng, X. Zhou, C. L. Ren, H. H. Li and X. G. Chen, *Anal. Chem.*, 2012, **84**, 5753–5758.